Article

Phosphatidylserine-Dependent Catalysis of Stalk and Pore Formation by Synaptobrevin JMR-TMD Peptide

Pradip K. Tarafdar,[1,2] Hirak Chakraborty,[1,2] Michael J. Bruno,[1,2] and Barry R. Lentz[1,2,*]

[1]Department of Biochemistry and Biophysics and [2]Molecular and Cellular Biophysics Program, University of North Carolina at Chapel Hill, Chapel Hill, North Carolina

ABSTRACT Although the importance of a SNARE complex in neurotransmitter release is widely accepted, there exist different views on how the complex promotes fusion. One hypothesis is that the SNARE complex's ability to bring membranes into contact is sufficient for fusion, another points to possible roles of juxtamembrane regions (JMRs) and transmembrane domains (TMDs) in catalyzing lipid rearrangement, and another notes the complex's presumed ability to bend membranes near the point of contact. Here, we performed experiments with highly curved vesicles brought into contact using low concentrations of polyethylene glycol (PEG) to investigate the influence of the synaptobrevin (SB) TMD with an attached JMR (SB-JMR-TMD) on the rates of stalk and pore formation during vesicle fusion. SB-JMR-TMD enhanced the rates of stalk and fusion pore (FP) formation in a sharply sigmoidal fashion. We observed an optimal influence at an average of three peptides per vesicle, but only with phosphatidylserine (PS)-containing vesicles. Approximately three SB-JMR-TMDs per vesicle optimally ordered the bilayer interior and excluded water in a similar sigmoidal fashion. The catalytic influences of hexadecane and SB-JMR-TMD on fusion kinetics showed little in common, suggesting different mechanisms. Both kinetic and membrane structure measurements support the hypotheses that SB-JMR-TMD 1) catalyzes initial intermediate formation as a result of its basic JMR disrupting ordered interbilayer water and permitting closer interbilayer approach, and 2) catalyzes pore formation by forming a membrane-spanning complex that increases curvature stress at the circumference of the hemifused diaphragm of the prepore intermediate state.

INTRODUCTION

Biological membrane fusion is observed in many vital intra- and intercellular events, including viral infection, neurotransmission, protein trafficking, and fertilization. During neuronal exocytosis, synaptic vesicles dock with the presynaptic plasma membranes and subsequently fuse to release entrapped neurotransmitters. Three soluble *N*-ethyl-maleimide sensitive factor attachment receptor proteins (SNAREs)—synaptobrevin (SB), located in the synaptic vesicle membrane, and syntaxin (SX) and SNAP-25 (SN25), located in the presynaptic membrane (1)—are key to this process. Although the importance of SNAREs for synaptic vesicles release is widely accepted, the molecular mechanism by which SNAREs might promote fusion remains unresolved. Residues K_{83}–K_{94} form a juxtamembrane region (JMR) that links the SNARE motif and the transmembrane domain (TMD) of SB, and have been suggested to regulate SNARE-mediated fusion (2,3). Apart from the JMR, the SNARE TMDs are critical for fusion (4-10). Multimers of syntaxin-1A TMDs have been reported to be essential for fusion pore (FP) formation (10), and a similar claim was made based on a recent mutational analysis of the SB-TMD (11). The SB-TMD has been reported to form homodimers in a sequence-specific manner, although the stability of the dimer is in question (12,13). Other studies have suggested that TMDs may somehow perturb the bilayer to promote or catalyze fusion (11,14,15). A crystal structure of a four-helix bundle of the SNARE motifs of SX-1A, SB-2, and SN-25B (16) led to the predominant view that zippering of SNAREs provides free energy for pulling membranes into close contact and bending them to promote fusion (17,18), as has been reported for model membranes (19). Here, we used low concentrations of polyethylene glycol (PEG) to bring highly curved small unilamellar vesicles (SUVs) into sufficiently close contact for fusion (20). In this way, we sought to determine the influence of the membrane-contacting regions of the vesicle-associated SNARE protein SB on fusion.

Fusion appears to be a multistep process, whether viewed by ensemble kinetics (21,22) or by recordings of individual fusion events (23,24). Ensemble kinetic measurements suggest at least one and sometimes two fusion intermediates, and predict a fast process followed by a 10-fold slower event (21,22,25-27). Likewise, analyses of multiple single fusion events in model systems have revealed processes that occur with two mean dwell times, with one process being roughly 10 times faster than the slowest one (23,24). Our ensemble

Submitted December 16, 2014, and accepted for publication August 26, 2015.

*Correspondence: uncbrl@gmail.com

Pradip K. Tarafdar's present address is Department of Chemical Sciences, Indian Institute of Science Education and Research Kolkata, Mohanpur, India.

Hirak Chakraborty's present address is School of Chemistry, Sambalpur University, Jyoti Vihar, Burla, India.

Editor: Axel Brunger.

0006-3495/15/11/1863/10

http://dx.doi.org/10.1016/j.bpj.2015.08.051

kinetic model envisions a rapidly formed initial aggregated state (state A), one or two intermediate states (stalk-like I_1 and expanded diaphragm-like I_2), and a final FP state. A simple model that views fusion in terms of evolution through thermodynamic intermediate states describes fusion kinetics in many disparate systems (22,25-29). Fig. S2 (in the Supporting Material) illustrates this model in terms of a calculated free-energy path between these geometries along a presumed stalk radius (30). An analysis of ensemble kinetic data obtained at multiple temperatures provides the transition-state thermodynamics (26), which offers mechanistic insights into how fusion proteins may alter individual steps of the fusion process.

Because phosphatidylserine (PS) is a significant component of synaptic vesicles (31) and has a significant influence on fusion in a Ca^{2+}-dependent fashion (29), we asked whether it might specifically impact the effect of SB-JMR-TMD on fusion. A global analysis of fluorescence data that reflect content mixing (CM), lipid mixing (LM), and leakage (L) provides both the kinetic parameters and activation thermodynamics for time evolution of the thermodynamic states leading to FP formation. By recording the influence of SB-JMR-TMD on fusion kinetics and SUV bilayer structure, we show that an average of three SB-JMR-TMD peptides per vesicle optimally catalyze both stalk and pore formation in a fashion that depends on the presence of PS.

MATERIALS AND METHODS

The materials and methods used in this work are briefly summarized in Supporting Materials and Methods.

Preparation of SB-JMR-TMD peptide and peptide-lipid model membranes

A 34-amino-acid region of the C-terminus of SB (K_{83}–T_{116}, sequence H- K_{83}LKRKYWW$_{90}$KNLK$_{94}$MMIILG$_{100}$VICAIILIII1$_{111}$VYFST$_{116}$-OH) containing a nonpolar string of 22 nonpolar amino acids (M_{95}–T_{116}, TMD) and a proximal positively charged region (K_{83}–K_{94}, JMR) was chemically synthesized and purified by Invitrogen (Carlsbad, CA). The peptide was dissolved in trifluoroethanol and water (90:10, v/v) and added to the appropriate lipid mixtures dissolved in chloroform to varying final [peptide]/[lipid] ratios. The solvent was removed by a nitrogen stream and the residue was dissolved in cyclohexane, followed by lyophilization to a dry white powder. After the dried peptide-lipid powder was suspended in the appropriate buffer, SUVs were prepared from DOPC/DOPE/SM/CH/DOPS (32:25:15:20:8 molar ratio), DOPC/DOPE/SM/CH/DOPG (32:25:15:20:8 molar ratio), and DOPC/DOPE/SM/CH (40:25:15:20 molar ratio) lipid mixtures using a titanium-probe sonication method (see Supporting Materials and Methods).

Recording and analyzing the fusion time courses, and calculating the activation thermodynamics

We recorded the time courses of LM and CM between vesicles using fluorescent probes as described in Supporting Materials and Methods, and in detail elsewhere (27). Our analysis globally fits all fluorescence measurements without making assumptions about the ultimate extents of LM, CM, or L, which instead are established by a global analysis in terms of an appropriate set of linked rate equations (22,26). For this reason, we cannot estimate rate constants directly from fluorescence measurements by assuming the total extents of CM or LM, as has normally been done in the past (32,33). Our ensemble kinetic measurements and analysis have been thoroughly vetted and are well documented (22,25,27,29), and a brief summary of both is given in Supporting Materials and Methods.

Effect of SB JMR-TMD on SUV bilayer properties

We used three fluorescent probes to record the influence of the JMR-TMD peptide on SUV bilayer structure. First, we employed C_6-NBD-phosphatidylcholine (PC) to report the free volume in and water penetration into the upper regions of the exposed SUV bilayer as described in Supporting Materials and Methods(34). Diphenylhexatriene (DPH) reports the average order in the acyl-chain region of the bilayer (35), and trimethylammonium (TMA)-DPH reports the average order in the upper region of the bilayer near the interface as well as water penetration into the interface (34).

RESULTS

Fusion of DOPS-containing SUVs with and without SB-JMR-TMD

We have measured the time courses of LM, CM, and L resulting from fusion of control DOPS-containing SUVS in presence of 6% (w/w) PEG at 23°C (Fig. S3). We previously showed that either a single-intermediate or a two-intermediate sequential model could describe all similar time courses for a variety of membrane compositions and conditions (25,27,35). For the lipid compositions examined here, we were able to globally describe all three kinetic data sets obtained at different peptide contents and temperatures using a single-intermediate ensemble kinetic model (see "Analysis of fusion time courses in terms of an ensemble kinetic model" in Supporting Materials and Methods). This provided the average rate constants for conversion between states (k_1 for intermediate formation and k_3 for pore formation) as well as the probabilities that microstructures that permit LM (β) and CM (α) exist in the intermediate ensemble state (22,26) (parameters are presented in the first row of Table S1; data from four other temperatures are provided in the bottom rows). The parameters k_1, β, and f_{LM} at 23°C were much reduced relative to values reported for similar vesicles lacking DOPS (see Table 1 of Sengupta et al. (35)). However, these parameters increased dramatically at 37°C in DOPS vesicles to values comparable to those observed at 23°C in the absence of DOPS (35), indicating that increased thermal energy can overcome DOPS inhibition of intermediate formation. Consistent with this observation, inhibition of close bilayer approach has been proposed to result from anionic repulsion or from PS-specific steric effects (29). At all temperatures, the extents of LM were greater than the extents of CM, meaning that not all membrane-bridging or hemifusion microstructures in intermediate I lead to transient or final pore formation. This is implied by the finite probability of CM in I-state (α).

The increase in α with temperature implies that some CM in I-state is associated with thermally triggered microstructural fluctuations (26).

Data were also collected over a range of peptide/lipid ratios for DOPS SUVs containing SB-JMR-TMD peptides (peptide content increases from the *bottom to top curves* in Fig. S3). Parameters obtained by analyzing these data are presented in Table S2. To visualize how peptide content influences fusion of PS-containing vesicles, we plot in Fig. 1 peptide-triggered changes (Δ values, with peptide-free reference values given in Table S3) in rate constants k_1 and k_3 (Fig. 1, *A* and *B*), probabilities β (Fig. 1 *C*), α (Fig. 1 *D*), and total extents of LM (%LM; Fig. 1 *E*) and CM (%CM; Fig. 1 *F*). The dependence of Δk_1 and Δk_3 on the mole fraction of SB-JMR-TMD for fusion of PS-containing vesicles (*solid circles*) was well described by a sharp sigmoidal curve rising above 0 at an ~0.0004 mole fraction and leveling at a mole fraction of ~0.0010–0.0012 peptide (roughly three peptides per vesicle; see Discussion). The rate constants remained constant above this peptide mole fraction. No other kinetic parameters showed this behavior, and the extents of LM (Fig. 1, *C* and *E*) and CM (Fig. 1, *D* and *F*) continued to increase with increased peptide content beyond three per vesicle.

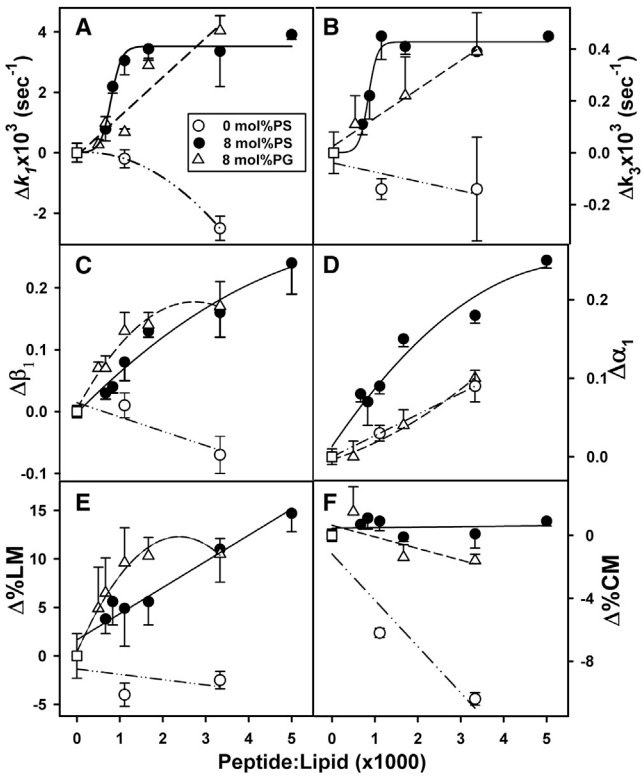

FIGURE 1 (*A–F*) Effects of SB-JMR-TMD on the rates of individual steps of fusion (*A* and *B*), the probabilities of LM (*C*) and CM (*D*) in the intermediate state, and the extents of LM (*E*) and CM (*F*). The total lipid concentration was 0.2 mM, temperature was 23°C, and the lipid compositions were DOPC/DOPE/SM/CH/DOPS (32:25:15:20:8 molar ratio, *solid circle*), DOPC/DOPE/SM/CH/DOPG (32:25:15:20:8 molar ratio, Δ), and DOPC/DOPE/SM/CH (40:25:15:20 molar ratio, *open circle*). Experiments performed on different days with different sample preparations were reproducible. At least two time courses were obtained each day for each sample, and the process was repeated when these data sets were not consistent. The parameter uncertainties shown here and in Tables S1–S4 and S6 were determined by averaging parameters obtained by analyzing at least three time courses collected on each of 3 days with freshly prepared samples. Parameters from individual analyses generally fell within these error bounds, as expected for a normal distribution. The curves drawn derive from fitting to standard sigmoid, linear, and quadratic equations.

Fusion of SB-JMR-TMD reconstituted in SUVs containing DOPG or DOPC

To determine whether the sigmoidal behaviors of k_1 and k_3 in Fig. 1 required PS, we collected kinetic data at 23°C for SUVs containing DOPC (see right frame of Fig. S3) or DOPG in place of DOPS (data not shown). Peptide-triggered changes in kinetic parameters for these lipid compositions are also plotted in Fig. 1 (*open triangles* for DOPG; *open circles* for DOPC), and reference quantities from peptide-free SUVs are given in Table S3. In the absence of acidic lipid (i.e., DOPC SUVs), the SB-JMR-TMD peptide inhibited rates for both steps of fusion (*open circles* in Fig. 1, *A* and *B*) as well as the extents of CM and LM (Fig. 1, *E* and *F*). Both acidic lipids relieved inhibition and permitted peptide-induced promotion of rates and extents, but promotion of pore formation in the intermediate state was greatest with DOPS. For DOPG-containing SUVs, rates increased in a roughly linear fashion with SB-JMR-TMD content, not in the sigmoidal fashion seen for PS-containing SUVs. LM extent in the intermediate state increased and then decreased with peptide content for DOPG, but increased without apparent limit for DOPS (Fig. 1, *C* and *E*). Similarly, peptide influence on pore formation in the intermediate state was greatest for PS SUVs (Fig. 1 *D*). We conclude that the influence of the SB-JMR-TMD peptide on PEG-mediated fusion depends on the lipid environment and is optimal for PS-containing SUVs.

Location of SB-JMR-TMD in the bilayer

The orientation of the SB-JMR-TMD across the bilayer of DOPS-SUVs at a peptide/lipid ratio of 1:300 was determined by potassium iodide (KI) quenching of the two Trp residues located close to the peptide N-terminal JMR (see Materials and Methods). Quenching was monitored and shown to be diffusional for peptide in membranes and in lipid/$C_{12}E_8$ mixed micelles (Fig. 2). The Stern-Volmer constants in the absence and presence of sufficient detergent to fully disrupt the SUVs (full content release) were comparable, i.e., JMR tryptophans were equally accessible to added KI in both intact and detergent-disrupted SUVs. There was no indication of the negative curvature characteristic of hidden or unavailable populations of fluorophores, and plotting of the data in a modified Stern-Volmer fashion supported

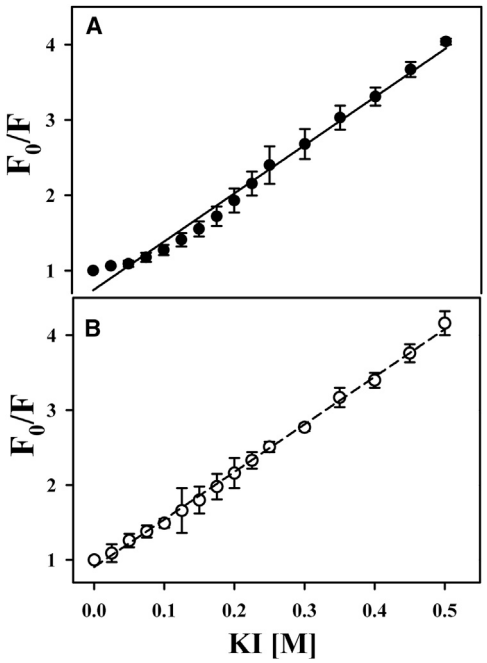

FIGURE 2 Quenching of SB-JMR-TMD Trp residues 89 and 90 with KI. (*A*) Titration of SB-JMR-TMD reconstituted into 200 μM DOPC/DOPE/SM/CH/DOPS (32:25:15:20:8) SUVs at a peptide/lipid ratio of 1:300 in 10 mM TES, 150 mM NaCl, 1 mM EDTA, and 1 mM Ca^{2+} buffer at pH 7.4. Triplicate measurements on each of three samples were averaged to obtain error bars. Linear regression through the data gave an average Stern-Volmer constant of 6.42 $\pm$ 0.20 M^{-1}. The slight positive curvature at low KI concentration in (*A*) can be attributed to correlated diffusion of I^- relative to the negatively charged membrane surface (36). (*B*) A similar titration using a reconstituted SUV preparation treated with 4.5 mM $C_{12}E_8$ yielded a Stern-Volmer constant of 6.35 $\pm$ 0.10 M^{-1}.

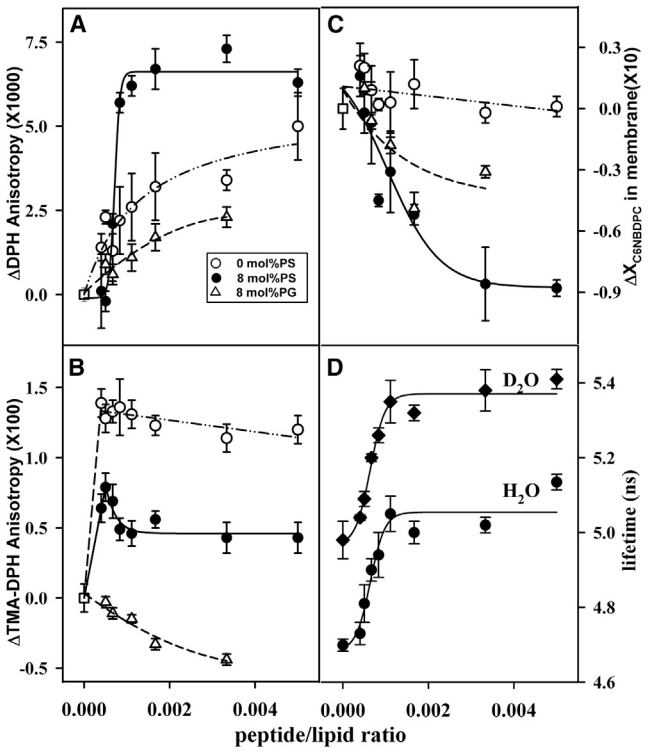

FIGURE 3 Effect of SB-JMR-TMD on SUV membrane properties. (*A*) Change with JMR-TMD mole fraction in acyl-chain order within SUVs as recorded in terms of the fluorescence anisotropy of the probe DPH. (*B*) Change with JMR-TMD mole fraction in the outer-leaflet interfacial order of SUVs as recorded in terms of the fluorescence anisotropy of the probe TMA-DPH. (*C*) Change with JMR-TMD mole fraction in partitioning of the probe C_6NBDPC into the SUV outer leaflet as a measure of outer-leaflet free volume. (*D*) TMA-DPH lifetime as observed in D_2O and H_2O as a function of the mole fraction of SB-TMD in SUVs composed of DOPC/DOPE/SM/CH/DOPS. Symbols and conditions are the same as in Fig. 1. The data in (*A*), (*C*), and (*D*) were fit to sigmoidal or hyperbolic curves to obtain the lines through these data. For (*B*), the increase and subsequent decrease in TMA-DPH anisotropy observed for DOPC and DOPS-SUVs were fitted separately (linear followed by linear or exponential decay). The concentration of lipid was 0.2 mM. All values are the average of at least three measurements.

this. These data establish the asymmetric orientation of SB-JMR-TMD peptides across the membrane.

We recorded tryptophan fluorescence spectra to obtain insight into the influence of acidic lipids on JMR-TMD peptide placement in the membrane. The results in Fig. S4 show that the Trp residues in the JMR are less exposed to water in membranes containing acidic lipids.

Influence of SB-JMR-TMD on bilayer structure

As expected for a transmembrane helix, SB-JMR-TMD produced increased average acyl-chain order in SUVs (DPH fluorescence anisotropy in Fig. 3 *A*). This increase was sharply sigmoidal up to an ~0.001 mole fraction for DOPS SUVs (●). Surprisingly, DPH fluorescence anisotropy did not increase upon inclusion of a >0.0011 mole fraction of SB-JMR-TMD in DOPS SUVs, a phenomenon that was not seen for DOPC and DOPG (○ and Δ, respectively). TMA-DPH anisotropy reflects the average order in the upper region of the bilayer that is occupied by this probe (34,37). This measure of order increased quite dramatically up to an ~0.0004 mole fraction (~1–1.3 peptides per vesicle) in DOPC-SUVs (Fig. 3 *B*, *open circles*), indicating that a single peptide is sufficient to dramatically order the interface in neutral-lipid SUVs, whereas additional peptide did not significantly increase order. Surprisingly, SB-JMR-TMD peptides disordered the interface in DOPG-containing SUVs (Δ), but ordered it in DOPS SUVs up to an ~0.0005 peptide mole fraction (~1.4–1.9 peptide per vesicle). Additional peptide disordered the interface relative to this maximum effect up to ~0.0011–0.0012 mole fraction.

The fraction of C_6NBD-PC ($X_{C6NBDPC}$) in a bilayer reflects the free volume available in the upper region of the bilayer to accommodate the probe (34). Increasing the SB-JMR-TMD peptide membrane content in DOPS or DOPG SUVs decreased $X_{C6NBDPC}$ dramatically (● and Δ, Fig. 3 *C*), with saturation at an ~0.003–0.004 mole fraction of peptide (the greater effect was observed with DOPS). SB-JMR-TMD had a minimal (if any) effect on DOPC-SUVs (○),

so acidic lipid seems to be critical for the ability of the peptide to reduce the membrane free volume, consistent with Trp residues partitioning deeper into the interface of acidic-lipid-containing SUVs (Fig. S4).

Effect of SB-JMR-TMD on the activation thermodynamics of PS-containing SUVs

The activation free energies, ΔG_1^* and ΔG_3^* refer to the differences in free energy between the initial states (A and I) and transition states for I and FP formation, respectively, according to the kinetic scheme provided in Supporting Materials and Methods under "Analysis of fusion time courses in terms of an ensemble kinetic model". These transition states are labeled TS1 (step 1) and TS3 (step 3) in the cartoon in Fig. S2. Fig. 4 *A* (*inset*) shows the temperature dependence of activation free energy for step 1 (ΔG_1^*) for control vesicles (i.e., absent peptide) obtained from measured rate constants at five fixed temperatures (23°C, 28°C, 33°C, 37°C, and 40°C) as described in Supporting Materials and Methods.

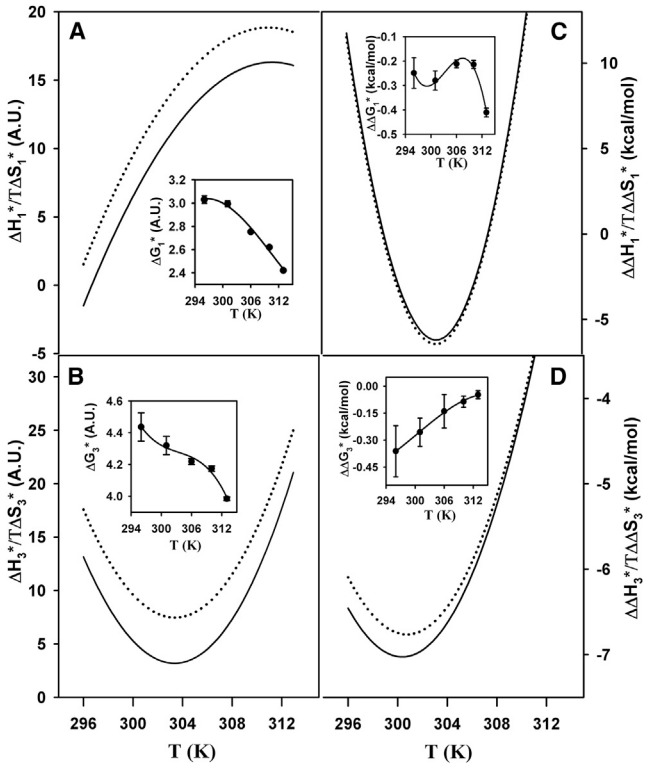

FIGURE 4 Effects of SB peptide on the activation barrier for different steps of PEG-induced fusion of DOPC/DOPE/SM/CH/DOPS SUVs. (*Left panel*) Temperature dependence of $T\Delta S_i^*$ (*solid line*) and ΔH_i^* (*dotted line*) for formation of the (*A*) I_1 state and (*B*) FP state during fusion of control vesicles. The insets show the activation free energy (ΔG_i^*) for these steps. (*C* and *D*) Changes in ΔH_i^* ($\Delta\Delta H_i^*$, *dotted line*) and $T\Delta S_i^*$ ($T\Delta\Delta S_i^*$, *solid line*) associated with inclusion of SB-JMR-TMD (peptide/lipid ratio 1:900) for (*C*) I_1 formation and (*D*) FP formation, with insets showing $\Delta\Delta G_i$. Expressions for ΔG_i^* and other values are provided in Materials and Methods, and coefficient values are given in Table S5.

ΔG_1^* was nonlinear in reciprocal temperature (i.e., the behavior was non-Arrhenius), and the activation enthalpy (and entropy) thus varied with temperature. Fig. 4 *B* (*inset*) shows the similarly non-Arrhenius activation free energy for step 3 (ΔG_3^*). As noted previously (25), cubic polynomials offer a thermodynamically and mathematically satisfactory empirical description of the temperature variation of both activation free energies (for the polynomial coefficients, see Table S5). We obtained the temperature dependencies of activation entropy ($T\Delta S_i^*$; *solid lines*) and enthalpy (ΔH_i^*; *dotted lines*) contributions (Fig. 4, *A* and *B*) by taking the appropriate temperature derivatives (see Supporting Materials and Methods and the legend to Table S5) (26) of the fitted ΔG_i^* curves. These values show that both steps are entropically permitted, i.e., a large positive ΔH_i^* is partially overcome by a large positive $T\Delta S_i^*$ (26). We similarly calculated the activation thermodynamics for fusion of SB-JMR-TMD peptide-containing DOPS SUVs at the peptide mole fraction (0.0011) that defined the optimal changes in k_1 and k_3 (Fig. 1, *A* and *B*), DPH fluorescence anisotropy (Fig. 3 *A*), and TMA-DPH fluorescence lifetimes (Fig. 3 *D*). From these results and those obtained for control SUVs, we determined the peptide-induced changes in activation free energy ($\Delta\Delta G_i^* = \Delta G_{i,peptide}^* - \Delta G_{i,control}^*$) recorded in the insets to Fig. 4, *C* and *D*. These small but clearly measurable activation free energies result from large compensating changes in activation enthalpy ($\Delta\Delta H_i^*$, *dotted lines*) and entropy ($\Delta\Delta S_i^*$, *solid lines*), which are plotted in the main sections of Fig. 4, *C* (I formation) and *D* (FP formation). These changes and $\Delta\Delta G_i^*$ depend on membrane curvature and on the interbilayer approach that we modulate with PEG concentration to keep the fusion kinetics in an experimentally accessible range. SB-JMR-TMD peptide catalysis of pore formation is enthalpically driven at all temperatures (Fig. 4 *D*), whereas catalysis of intermediate formation is more complicated, being enthalpically driven from 300 K to 308 K, and entropically driven above and below this range (Fig. 4 *C*). These results have implications for possible mechanisms of peptide-mediated catalysis, as will be discussed below.

Effects of SB-JMR-TMD versus 2 mol % hexadecane on PEG-mediated SUV fusion

Table S6 reports the effects of 2 mol % hexadecane on the kinetic parameters for PEG-mediated fusion of control (*solid circles*) and peptide-containing DOPS SUVs at 23°C and 37°C. Fig. 5 summarizes the influences of peptide (*dark gray squares*), hexadecane (*light gray triangles*), and hexadecane plus peptide (*gray diamonds*) on activation free energy. In the absence of peptide, hexadecane had little effect on the activation free energy of intermediate formation (ΔG^*_1) (Fig. 5 *A*). It increased both the rate of pore formation (k_3) and extent of CM (%CM) modestly (ΔG^*_3 in Fig. 5 *B* and Table S6), and it increased somewhat more

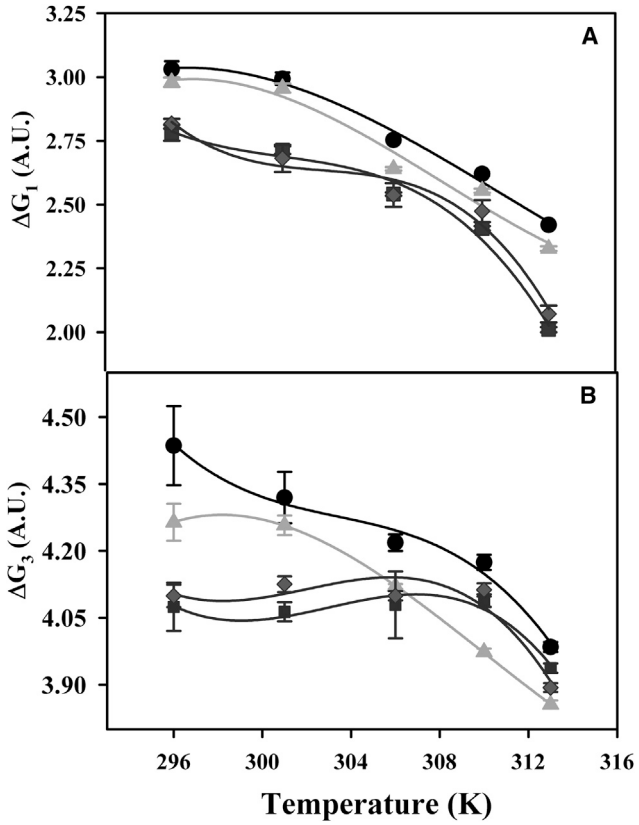

FIGURE 5 (*A* and *B*) Temperature dependence of the free-energy barrier for formation of the (*A*) I state and (*B*) FP state for control vesicles (*solid circle*), vesicles in the presence of SB-JMR-TMD peptide (*solid box*), vesicles containing 2 mol % hexadecane (*light gray triangle*), and vesicles containing 2 mol % hexadecane in the presence of SB-JMR-TMD (*dark gray diamond*). L/P ratio 900:1; vesicles composed of DOPC/DOPE/SM/CH/DOPS, 32:25:15:20:8 molar ratio.

dramatically the extent of CM in the initial stage of fusion (α) (Table S6). In a previous study (35), we showed that hexadecane had somewhat larger effects on membranes lacking PS: it increased k_1 by ~24–26% and increased %CM by 50% and 30% at 23°C and 37°C, respectively. Of greatest interest here, however, was the combined influence of the SB-JMR-TMD peptide and hexadecane (*dark gray diamonds* in Fig. 5). Adding hexadecane to SUVs containing peptide hardly influenced the rates of intermediate (k_1) or pore (k_3) formation, and thus ΔG^*_1 and ΔG^*_3. The lack of cooperative influences of hexadecane and SB-JMR-TMD peptide implies that hexadecane and peptide do not share a catalytic mechanism.

DISCUSSION

SB-JMR-TMD peptides cooperatively produce local structural changes that enhance fusion in PS-containing SUVs

The sigmoidal influence of SB JMR-TMD peptide on k_1 and k_3 (Fig. 1, *A* and *B*), DPH anisotropy (Fig. 3 *A*), and TMA-DPH fluorescence lifetime (Fig. 3 *D*) can most reasonably be interpreted in terms of a peptide or peptide/lipid complex influencing both membrane structure and SUV fusion. The potential implications of such an interpretation are evident in the literature on SNARE-mediated fusion. There is considerable disagreement as to whether one (38), two or three (39,40), or up to eight or 10 SNARE complexes (41,42) might be required for SNARE-mediated fusion. Although there is some evidence that clustering of SX in both model and secretory membranes promotes fusion (10,43), there is disagreement over whether SB-TMDs might form multimers in a membrane. In one study, investigators used ToxR analysis and chimeric proteins containing four different hydrophobic portions of SB-TMD to test for multimer formation in a membrane, and found none (12). In another study, researchers used the same technology with chimeras containing a different hydrophobic sequence and reported the detection of dimers (13). These contrasting reports fail to clarify whether the SB-TMD might form multimers in a membrane. Instead of using just SB-TMD, we included the basic JMR in our synthetic peptide (SB-JMR-TMD) because of the important roles that have been assigned to the JMR in model-system fusion (44,45). We documented PS-requiring structural and catalytic effects of SB-JMR-TMD peptides reconstituted in a directed fashion into SUVs at roughly three per vesicle.

How many peptides are required for optimal PEG-mediated fusion of vesicles containing PS? The surface area of fluid-phase PCs is roughly 65–70 Å^2, whereas phosphatidylethanolamines have smaller surface areas. PS is larger and cholesterol fits in between phospholipid molecules. SUV outer leaflets have surface areas roughly twice as large as their inner leaflets, and the hydrodynamic radii of our PS-containing vesicles are ~26 nm. Taking all of these observations into account, we estimate that each SUV should contain between 2500 and 3300 lipids. Saturation of k_1 and k_3 was reached at an ~0.0011 mole fraction of JMR-TMD or ~900 lipids/JMR-TMD. Thus, fusion rates saturated when 2.8–3.6 peptides were incorporated into each vesicle, assuming that the peptides were randomly distributed between vesicles during reconstitution.

How can we explain this stepwise or cooperative behavior? We can rule out the possibility that DOPS-SUVs become unstable and prone to fuse above three peptides per vesicle, since we observed that our SUV preparations remained small, monodisperse, and nonleaky over the full range of peptide content investigated. We observed continuous variation of both membrane structural properties and kinetics of fusion events over a range of 0 to 12–16 peptides per SUV for all lipid compositions, thus eliminating the possibility that a maximum of three peptides can be incorporated into SUVs. Therefore, we hypothesize that some sort of peptide or peptide-lipid complex containing roughly three peptides catalyzes fusion. If so, why does catalysis not change with increasing peptide mole fractions

beyond 0.0011 as multiple complexes form? We believe this is a consequence of rapid lateral diffusion of proteins and lipids in the bilayer ($D^{(2)}$ ~10^{-8} cm^2/s (46)). Fusion must occur at a point of contact between SUVs. A hypothetical SB-JMR-TMD trimer would sample a point of contact between SUVs roughly 10–13 times per second. The ensemble averaged constants k_1 and k_3 are 3–4 orders of magnitude slower, so the rate-limiting step in fusion is not diffusion of the peptide catalyst into the fusing region, but rather the millisecond rates associated with intermediate or pore formation. This makes it immaterial whether an SUV contains one, two, three, or more complexes.

Measures of membrane order or water penetration obtained with DPH or TMA-DPH also showed stepwise changes with the peptide mole fraction. As detailed in Supporting Materials and Methods, DPH appears to partition equally between different membrane microenvironments, and its anisotropy is an intensity- and mole-fraction-weighted average over these microenvironments. If we assume a reasonable value for the anisotropy in an ordered peptide-lipid complex, this equipartition model implies weak assemblages of roughly three peptides with many lipids (approximately seven lipid layers). Alternatively, we could explain our data by abandoning this model and assuming that DPH probes partition preferentially into one or two lipid layers near a tight peptide complex. Both models suggest that DPH probes reflect locally increased lipid order. For these models, the lipids associated with a peptide complex would be 0.3–0.9% of the total lipids. DPH anisotropy reaches an optimal and steady value at one peptide/lipid complex per vesicle (Fig. 3 *A*). Because errors in DPH anisotropy changes are ~5%, the difference between one and three peptide/lipid complexes per SUV cannot be distinguished within error.

In contrast to the step-like changes detected by DPH or TMA-DPH, the membrane free volume as reported by C_6NBD-PC partitioning decreased monotonically with the peptide mole fraction (Fig. 3 *C*). This presumably is because the free volume reflects a global membrane property (roughly surface tension) rather than local changes.

Specific role of PS in SB-JMR-TMD catalysis of fusion

Although we do not know the exact nature of the peptide complex suggested by our results, inclusion of DOPS in a membrane produced effects that were not seen with DOPC or DOPG. TMA-DPH anisotropy (Fig. 3 *B*) suggests that a JMR-TMD monomer predominates in DOPC SUVs. This conformation had little effect on the membrane free volume (Fig. 3 *C*), was anticatalytic, and inhibited pore formation (Fig. 1). JMR Trp fluorescence increased (Fig. S4), free volume was reduced (Fig. 3 *C*), and fusion was enhanced (Fig. 1) in the presence of both DOPG and DOPS. This is consistent with an acidic-lipid-induced, nonspecific conformational shift burying the peptide and possibly relieving monomer steric interference with bilayer close approach and fusion (Fig. 1). It may be that specific binding of PS to a regulatory site (47-49) on the JMR allosterically regulates the TMD structure so as to expose a protein-protein interaction motif that triggers the development of peptide complexes. If so, the interaction free energy leading to a complex might be strong enough to be estimated and should depend on PS content. Alternatively, interaction of the PS amine with the electronic distribution of Trp residues (50,51) might alter the TMD orientation in the bilayer and modify lipid packing, thereby resulting in a thermodynamic packing force that favors the separation of a protein-lipid complex from lipid-rich regions (52,53). One might be able to investigate these possibilities by using fluorescently labeled peptides to determine association constants for complex formation, but this would require experimentation well beyond the scope of this study.

Structural information about JMR-TMD is consistent with either possibility. A hydrophobic region (beginning at the Trp pair) of a JMR-TMD construct (L^{79}–Y^{112}FST versus K^{83}–Y^{112}FST for our construct) has been proposed to form a transmembrane helix in neutral lipid bilayers (54). A previous NMR and electron paramagnetic resonance examination of SB residues 36–116 in the presence of dodecylphosphocholine (DPC) micelles identified an amphipathic helix (residues 36–54), a long unstructured region (residues 55–76), a small transient helix (residues 77–88) corresponding to the JMR, and a stable helix (L_{93}–T_{116}) corresponding to the TMD (55). Although the helical nature of the TMD was clearly established by that study, another study found that its orientation in a bilayer was more difficult to establish because of possible imperfections in deposited lipid bilayers (54), and another reported that DPC micelles cannot be assumed to mimic bilayers (55). The more plastic JMR structure suggests that it could be the source of allosteric regulation of TMD structure or orientation in the bilayer. Mutation of basic amino acid residues in this domain might be useful for sorting this out. As noted above, the stepwise influence of three peptides per vesicle (Figs. 1 and 3) and the asymmetric orientation of the JMR-TMD peptide across the bilayer (Fig. 2) bias us toward a trimer hypothesis. However, the following discussion of kinetic changes (Figs. S2 and 4) does not depend on the exact nature of the complex, but rather on its observed influences on local bilayer structure.

How might a SB-JMR-TMD complex catalyze fusion?

First step: initial intermediate or stalk formation

The catalytic influence of SB-JMR-TMD on step 1 varied significantly with temperature (Fig. 4 *C*): it was entropic at the lowest and highest temperatures ($T\Delta\Delta S_1^* > \Delta\Delta H_1^* > 0$)

and enthalpic at intermediate temperatures ($\Delta\Delta H_1^* < T\Delta\Delta S_1^* < 0$), with $\Delta\Delta Cp_1$ varying from negative to positive over this temperature range (27). PS inhibits initial intermediate formation between PEG-aggregated SUVs (29). We proposed that this inhibition may reflect electrostatic repulsion between PS-containing monolayers as well as hydrogen (H)-bond-induced ordering of the PS headgroup and associated water (56,57), with both influences preventing close approach of the bilayer in state A. We previously suggested that Ca^{2+} mediates against both of these influences to promote fusion (29). The basic JMR could have similar influences on bilayer-bilayer approach and interfacial order. Entropic catalysis at low temperatures implies a loss of entropy in state A or an increase in TS1, or both. The large negative $\Delta\Delta Cp_1^*$ at low temperature suggests an influence of the JMR-TMD on water structure in the A state. Although no molecular-dynamics simulations of the JMR adjacent to PS-containing membranes have been reported to date, the basic JMR of our synthetic peptide should relax the reported rigidifying influence of PS on water molecules to favor the type of weakly ordered water that is more characteristic of PC hydration (58). Weaker water ordering in state A would be consistent with the observed entropic catalysis and negative $\Delta\Delta Cp_1^*$ at low temperatures, where weak water-water H-bonds would give the A state a positive structural heat capacity that would be lost in TS1. We must also look at potential influences of the peptide on TS1. Bilayer structure measurements indicate that the peptide complex orders the bilayer and inhibits water entry into the interface region. We have proposed that similar influences of hemagglutinin fusion peptide make the acyl-chain excursion into the interbilayer space that is thought to occur in TS1 less enthalpically unfavorable (27). This could explain the switch to enthalpic catalysis ($\Delta\Delta H_1^* < T\Delta\Delta S_1^* < 0$) as the influence of weakly structured water in state A wanes with temperature. The observed entropic catalysis at higher temperatures ($T\Delta\Delta S_1^* > \Delta\Delta H_1^* > 0$) and a positive $\Delta\Delta Cp_1^*$ (Fig. 4 *C*) suggest that the JMR-TMD peptide at higher temperatures either broadens the distribution of closely spaced, energetically unfavorable states in TS1 or orders the A state. The acyl-chain-ordering influence of the peptide should decrease with temperature, as previously observed for fusion peptide (27), so we consider how the SB-JMR-TMD peptide might influence TS1 with increasing temperature. Acyl-chain excursions into the interbilayer space have previously been proposed for TS1 (26,59,60). These should make it an entropically favored state that would play a larger role in activation thermodynamics with increasing temperature. If the basic JMR-TMD disrupts PS-PS and PS-water H-bonding (57), this would broaden the TS1 microstructural ensemble at all temperatures and further enhance entropic catalysis at high temperature. In summary, we suggest that the catalytic influence of the JMR-TMD complex can be explained both by the ability of the TMD to fill space and order the bilayer, and by the basic charge of the JMR, with the relative influences of these effects varying with temperature. Aspects of this hypothesis are illustrated in the cartoon in Fig. S5.

Final step: conversion from an intermediate to an FP state

A simple materials-based calculation estimates the free-energy path a pair of SUVs traverses from an initial stalk intermediate through diaphragm-like intermediates as a function of stalk radius (r_s; see Fig. S2) (30). Although we do not envision vesicles marching in unison along a well-defined structural pathway, collections of microstructures related to those predicted by these estimates and molecular-dynamics calculations (59,60) likely contribute to the thermodynamic intermediate states that should describe the ensemble fusion kinetics of PEG-aggregated SUVs. Fusion between PS-containing (used here) and PS-free SUVs (25) at pH 7.4 can be described by a two-step, single-intermediate process. This means that a semistable I_2 intermediate state, as depicted in Fig. S2, is likely too unstable to be detected, although FPs still likely arise from microstates with diaphragm-like geometries (Fig. S2) (25,30). Such structures are predicted to be unstable due to unfavorable interstice energy and extreme negative curvature at their diaphragm circumference (Fig. S2) (30). The geometry of the predicted transition state (TS3) from I_2 to an FP state differs from I_2 only in r_s. We have proposed that r_s increases from r_2 (or r_1 when I_2 is unstable) to a critical r_s (r_s*) beyond which lipid fluctuations in the intermediate circumference become so unfavorable and numerous that some unstable microstructures transform into pores (FP state). Within this view, there are two ways to promote pore formation (27): 1) reduce the interstice energy so that r_2 can increase to approach r_s* or 2) increase curvature stress at the circumference of diaphragm-like microstructures so that r_s* will move to smaller stalk radii. Hexadecane seems to act through the former mechanism, consistent with its documented ability to increase the extent of CM (%CM) (26,27), even in the presence of SB-JMR-TMD (Table S6). However, it is quite clear from Fig. 5 that hexadecane and SB-JMR-TMD do not have similar influences on either step of SUV fusion. Our membrane structure measurements indicate that the SB-JMR-TMD at three peptides per vesicle should contribute positive intrinsic curvature to the membrane leaflets. Since the diaphragm geometry of I_2 imposes a large negative curvature on both the merged *cis* and the unfused *trans* leaflets of I_2 (Fig. S2, *bottom inset*), we propose that the SB transmembrane helix destabilizes this geometry and moves r_s* to smaller stalk radii. This accounts for the observed enthalpic catalysis (Fig. 4 *D*, again illustrated in Fig. S5).

Catalytic roles of TMDs

Many reports have led to the predominant hypothesis that SNARE TMDs play an essential role in fusion (4); however, not all investigators agree with this hypothesis. Specifically,

it has been shown that one can sometimes partially overcome the loss of TMDs by providing an alternative means of bringing the membranes into close contact (14,15). In addition, it has been reported that multiple SNARE complexes promote faster fusion pore opening because more SNARE complexes are pulling on them (15,61). However, the results presented here offer a possible alternative view, i.e., that a complex of SNARE JMR-TMDs may catalyze both steps of the fusion process. It is difficult to judge the potential biological significance of such a complex from our in vitro experiments. First, our results cannot prove the existence of a tight complex. Second, the magnitudes of the changes we detect are small (only ~53% increase in k_1 and 85% increase in k_3 at 23°C). However, we measure ensemble-averaged rates, and we estimate that peptide complexes should occupy only ~0.1% of intervesicle contacts. Thus, the influence of a peptide complex on a discrete fusion event could be orders of magnitude larger than we can detect. Only single-event measurements can resolve this issue.

SUPPORTING MATERIAL

Supporting Materials and Methods, five figures, and six tables are available at http://www.biophysj.org/biophysj/supplemental/S0006-3495(15)00948-0.

AUTHOR CONTRIBUTIONS

P.K.T., B.R.L., and H.C. collaborated in the design of experiments. P.K.T. performed most of the experiments with some help from M.J.B. P.K.T. and H.C. wrote the draft manuscript, and P.K.T., B.R.L., and H.C. collaborated in preparing the final manuscript.

ACKNOWLEDGMENTS

We are indebted to three reviewers who kindly provided detailed and helpful comments and suggestions that allowed us to substantially improve our manuscript.

This work was supported by U.S. Public Health Service grant GM32707 to B.R.L.

REFERENCES

1. Söllner, T., S. W. Whiteheart, …, J. E. Rothman. 1993. SNAP receptors implicated in vesicle targeting and fusion. *Nature.* 362:318–324.
2. Kweon, D. H., C. S. Kim, and Y. K. Shin. 2003. Regulation of neuronal SNARE assembly by the membrane. *Nat. Struct. Biol.* 10:440–447.
3. Quetglas, S., C. Iborra, …, M. Seagar. 2002. Calmodulin and lipid binding to synaptobrevin regulates calcium-dependent exocytosis. *EMBO J.* 21:3970–3979.
4. Langosch, D., M. Hofmann, and C. Ungermann. 2007. The role of transmembrane domains in membrane fusion. *Cell. Mol. Life Sci.* 64:850–864.
5. McNew, J. A., T. Weber, …, J. E. Rothman. 2000. Close is not enough: SNARE-dependent membrane fusion requires an active mechanism that transduces force to membrane anchors. *J. Cell Biol.* 150:105–117.
6. Grote, E., M. Baba, …, P. J. Novick. 2000. Geranylgeranylated SNAREs are dominant inhibitors of membrane fusion. *J. Cell Biol.* 151:453–466.
7. Shi, L., Q. T. Shen, …, F. Pincet. 2012. SNARE proteins: one to fuse and three to keep the nascent fusion pore open. *Science.* 335:1355–1359.
8. Fdez, E., M. Martínez-Salvador, …, S. Hilfiker. 2010. Transmembrane-domain determinants for SNARE-mediated membrane fusion. *J. Cell Sci.* 123:2473–2480.
9. Ngatchou, A. N., K. Kisler, …, M. Lindau. 2010. Role of the synaptobrevin C terminus in fusion pore formation. *Proc. Natl. Acad. Sci. USA.* 107:18463–18468.
10. Han, X., C. T. Wang, …, M. B. Jackson. 2004. Transmembrane segments of syntaxin line the fusion pore of Ca^{2+}-triggered exocytosis. *Science.* 304:289–292.
11. Chang, C.-W., E. Hui, …, M. B. Jackson. 2015. A structural role for the synaptobrevin 2 transmembrane domain in dense-core vesicle fusion pores. *J. Neurosci.* 35:5772–5780.
12. Bowen, M. E., D. M. Engelman, and A. T. Brunger. 2002. Mutational analysis of synaptobrevin transmembrane domain oligomerization. *Biochemistry.* 41:15861–15866.
13. Roy, R., R. Laage, and D. Langosch. 2004. Synaptobrevin transmembrane domain dimerization-revisited. *Biochemistry.* 43:4964–4970.
14. Xu, H., M. Zick, …, Y. Jun. 2011. A lipid-anchored SNARE supports membrane fusion. *Proc. Natl. Acad. Sci. USA.* 108:17325–17330.
15. Zhou, P., T. Bacaj, …, T. C. Südhof. 2013. Lipid-anchored SNAREs lacking transmembrane regions fully support membrane fusion during neurotransmitter release. *Neuron.* 80:470–483.
16. Sutton, R. B., D. Fasshauer, …, A. T. Brunger. 1998. Crystal structure of a SNARE complex involved in synaptic exocytosis at 2.4 A resolution. *Nature.* 395:347–353, (see comments).
17. Lentz, B. R., V. Malinin, M. E. Haque, and K. Evans. 2000. Protein machines and lipid assemblies: current views of cell membrane fusion. *Curr Opin Struct Biol.* 10:607–615.
18. Kozlov, M. M., H. T. McMahon, and L. V. Chernomordik. 2010. Protein-driven membrane stresses in fusion and fission. *Trends Biochem. Sci.* 35:699–706.
19. Burgess, S. W., T. J. McIntosh, and B. R. Lentz. 1992. Modulation of poly(ethylene glycol)-induced fusion by membrane hydration: importance of interbilayer separation. *Biochemistry.* 31:2653–2661.
20. Lentz, B. R. 2007. PEG as a tool to gain insight into membrane fusion. *Eur. Biophys. J.* 36:315–326.
21. Lee, J., and B. R. Lentz. 1997. Evolution of lipidic structures during model membrane fusion and the relation of this process to cell membrane fusion. *Biochemistry.* 36:6251–6259.
22. Weinreb, G., and B. R. Lentz. 2007. Analysis of membrane fusion as a two-state sequential process: evaluation of the stalk model. *Biophys. J.* 92:4012–4029.
23. Yoon, T.-Y., B. Okumus, …, T. Ha. 2006. Multiple intermediates in SNARE-induced membrane fusion. *Proc. Natl. Acad. Sci. USA.* 103:19731–19736.
24. Kyoung, M., A. Srivastava, …, A. T. Brunger. 2011. In vitro system capable of differentiating fast Ca2+-triggered content mixing from lipid exchange for mechanistic studies of neurotransmitter release. *Proc. Natl. Acad. Sci. USA.* 108:E304–E313.
25. Chakraborty, H., T. Sengupta, and B. R. Lentz. 2014. pH Alters PEG-mediated fusion of phosphatidylethanolamine-containing vesicles. *Biophys. J.* 107:1327–1338.
26. Chakraborty, H., P. K. Tarafdar, …, B. R. Lentz. 2012. Activation thermodynamics of poly(ethylene glycol)-mediated model membrane fusion support mechanistic models of stalk and pore formation. *Biophys. J.* 102:2751–2760.
27. Chakraborty, H., P. K. Tarafdar, …, B. R. Lentz. 2013. Wild-type and mutant hemagglutinin fusion peptides alter bilayer structure as well as kinetics and activation thermodynamics of stalk and pore formation differently: mechanistic implications. *Biophys. J.* 105:2495–2506.

28. Haque, M. E., H. Chakraborty, …, B. R. Lentz. 2011. Hemagglutinin fusion peptide mutants in model membranes: structural properties, membrane physical properties, and PEG-mediated fusion. *Biophys. J.* 101:1095–1104.

29. Tarafdar, P. K., H. Chakraborty, …, B. R. Lentz. 2012. Phosphatidylserine inhibits and calcium promotes model membrane fusion. *Biophys. J.* 103:1880–1889.

30. Malinin, V. S., and B. R. Lentz. 2004. Energetics of vesicle fusion intermediates: comparison of calculations with observed effects of osmotic and curvature stresses. *Biophys. J.* 86:2951–2964.

31. Takamori, S., M. Holt, …, R. Jahn. 2006. Molecular anatomy of a trafficking organelle. *Cell.* 127:831–846.

32. Wilschut, J., J. Scholma, …, S. Nir. 1985. Ca^{2+}-induced fusion of phosphatidylserine vesicles: mass action kinetic analysis of membrane lipid mixing and aqueous contents mixing. *Biochim. Biophys. Acta.* 821:45–55.

33. Malinin, V. S., M. E. Haque, and B. R. Lentz. 2001. The rate of lipid transfer during fusion depends on the structure of fluorescent lipid probes: a new chain-labeled lipid transfer probe pair. *Biochemistry.* 40:8292–8299.

34. Lee, J., and B. R. Lentz. 1997. Outer leaflet-packing defects promote poly(ethylene glycol)-mediated fusion of large unilamellar vesicles. *Biochemistry.* 36:421–431.

35. Sengupta, T., H. Chakraborty, and B. R. Lentz. 2014. The transmembrane domain peptide of vesicular stomatitis virus promotes both intermediate and pore formation during PEG-mediated vesicle fusion. *Biophys. J.* 107:1318–1326.

36. Keizer, J. 1983. Non-linear fluorescence quenching and the origin of positive curvature in Stern-Volmer plots. *J. Am. Chem. Soc.* 105: 1494–1498.

37. Ho, C., S. J. Slater, and C. D. Stubbs. 1995. Hydration and order in lipid bilayers. *Biochemistry.* 34:6188–6195.

38. van den Bogaart, G., M. G. Holt, …, R. Jahn. 2010. One SNARE complex is sufficient for membrane fusion. *Nat. Struct. Mol. Biol.* 17: 358–364.

39. Sinha, R., S. Ahmed, …, J. Klingauf. 2011. Two synaptobrevin molecules are sufficient for vesicle fusion in central nervous system synapses. *Proc. Natl. Acad. Sci. USA.* 108:14318–14323.

40. Mohrmann, R., H. de Wit, …, J. B. Sørensen. 2010. Fast vesicle fusion in living cells requires at least three SNARE complexes. *Science.* 330:502–505.

41. Domanska, M. K., V. Kiessling, …, L. K. Tamm. 2009. Single vesicle millisecond fusion kinetics reveals number of SNARE complexes optimal for fast SNARE-mediated membrane fusion. *J. Biol. Chem.* 284:32158–32166.

42. Karatekin, E., J. Di Giovanni, …, J. E. Rothman. 2010. A fast, single-vesicle fusion assay mimics physiological SNARE requirements. *Proc. Natl. Acad. Sci. USA.* 107:3517–3521.

43. Murray, D. H., and L. K. Tamm. 2009. Clustering of syntaxin-1A in model membranes is modulated by phosphatidylinositol 4,5-bisphosphate and cholesterol. *Biochemistry.* 48:4617–4625.

44. McNew, J. A., T. Weber, …, J. E. Rothman. 1999. The length of the flexible SNAREpin juxtamembrane region is a critical determinant of SNARE-dependent fusion. *Mol. Cell.* 4:415–421.

45. Williams, D., J. Vicôgne, …, J. E. Pessin. 2009. Evidence that electrostatic interactions between vesicle-associated membrane protein 2 and acidic phospholipids may modulate the fusion of transport vesicles with the plasma membrane. *Mol. Biol. Cell.* 20:4910–4919.

46. Jacobson, K., A. Ishihara, and R. Inman. 1987. Lateral diffusion of proteins in membranes. *Annu. Rev. Physiol.* 49:163–175.

47. Conesa-Zamora, P., M. J. Lopez-Andreo, …, S. Corbalán-García. 2001. Identification of the phosphatidylserine binding site in the C2 domain that is important for PKC alpha activation and in vivo cell localization. *Biochemistry.* 40:13898–13905.

48. Srivastava, A., J. Wang, …, B. R. Lentz. 2002. Localization of phosphatidylserine binding sites to structural domains of factor Xa. *J. Biol. Chem.* 277:1855–1863.

49. Majumder, R., M. A. Quinn-Allen, …, B. R. Lentz. 2008. A phosphatidylserine binding site in factor Va C1 domain regulates both assembly and activity of the prothrombinase complex. *Blood.* 112:2795–2802.

50. Sanchez, K. M., G. Kang, …, J. E. Kim. 2011. Tryptophan-lipid interactions in membrane protein folding probed by ultraviolet resonance Raman and fluorescence spectroscopy. *Biophys. J.* 100:2121–2130.

51. Gaede, H. C., W. M. Yau, and K. Gawrisch. 2005. Electrostatic contributions to indole-lipid interactions. *J. Phys. Chem. B.* 109:13014–13023.

52. Lentz, B. R., K. W. Clubb, …, G. Meissner. 1985. Phase behavior of membranes reconstituted from dipentadecanoylphosphatidylcholine and the Mg^{2+}-dependent, Ca^{2+}-stimulated adenosinetriphosphatase of sarcoplasmic reticulum: evidence for a disrupted lipid domain surrounding protein. *Biochemistry.* 24:433–442.

53. Schäfer, L. V., D. H. de Jong, …, S. J. Marrink. 2011. Lipid packing drives the segregation of transmembrane helices into disordered lipid domains in model membranes. *Proc. Natl. Acad. Sci. USA.* 108:1343–1348.

54. Bowen, M., and A. T. Brunger. 2006. Conformation of the synaptobrevin transmembrane domain. *Proc. Natl. Acad. Sci. USA.* 103:8378–8383.

55. Ellena, J. F., B. Liang, …, L. K. Tamm. 2009. Dynamic structure of lipid-bound synaptobrevin suggests a nucleation-propagation mechanism for trans-SNARE complex formation. *Proc. Natl. Acad. Sci. USA.* 106:20306–20311.

56. Berkowitz, M. L., and S. A. Pandit. 2002. Molecular dynamics simulation of dipalmitoylphosphatidylserine bilayer with Na+ counterions. *Biophys. J.* 82:1818–1827.

57. Pandit, S. A., D. Bostick, and M. L. Berkowitz. 2003. Mixed bilayer containing dipalmitoylphosphatidylcholine and dipalmitoylphosphatidylserine: lipid complexation, ion binding, and electrostatics. *Biophys. J.* 85:3120–3131.

58. Perera, L., U. Essmann, and M. L. Berkowitz. 1996. Role of water in the hydration force acting between lipid bilayers. *Langmuir.* 12: 2625–2629.

59. Smirnova, Y. G., S. J. Marrink, …, V. Knecht. 2010. Solvent-exposed tails as prestalk transition states for membrane fusion at low hydration. *J. Am. Chem. Soc.* 132:6710–6718.

60. Kasson, P. M., E. Lindahl, and V. S. Pande. 2010. Atomic-resolution simulations predict a transition.

61. Acuna, C., Q. Guo, …, T. C. Südhof. 2014. Microsecond dissection of neurotransmitter release: SNARE-complex assembly dictates speed and Ca^{2+} sensitivity. *Neuron.* 82:1088–1100.